ARTICLE

Concentration-Dependent Effect of Nickel Ions on Amyloid Fibril Formation Kinetics of Hen Egg White Lysozyme: a Raman Spectroscopy Study

Xinfei Li, Xiaodong Chen, Ning Chen, Liming Liu, Xiaoguo Zhou*, Shilin Liu*

Department of Chemical Physics, University of Science and Technology of China, Hefei 230026, China

(Dated: Received on March 15, 2023; Accepted on April 28, 2023)

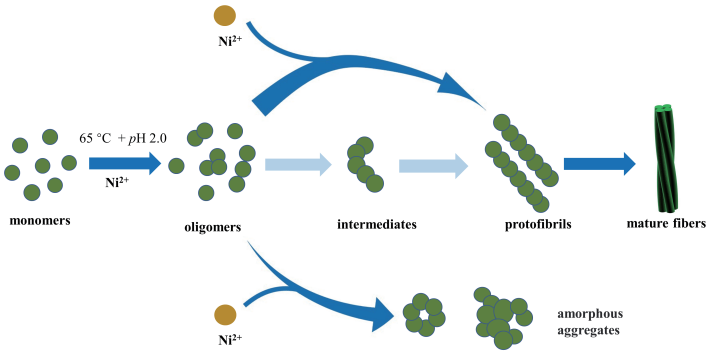

Nickel, an important transition metal element, is one of the trace elements for human body and has a crucial impact on life and health. Some evidences show the excess exposure to metal ions might be associated with neurological diseases. Herein, we applied Raman spectroscopy to study the Ni(II) ion effect on kinetics of amyloid fibrillation of hen egg white lysozyme (HEWL) in thermal and acidic conditions. Using the well-known Raman indicators for protein tertiary and secondary structures, we monitored and analyzed the concentration effect of Ni(II) ions on the unfolding of tertiary structures and the transformation of secondary structures. The experimental evidence validates the accelerator role of the metal ion in the kinetics. Notably, the additional analysis of the amide I band profile, combined with thioflavin-T fluorescence assays, clearly indicates the inhibitory effect of Ni(II) ions on the formation of amyloid fibrils with organized β-sheets structures. Instead, a more significant promotion influence is affirmed on the assembly into other aggregates with disordered structures. The present results provide rich information about the specific metal-mediated protein fibrillation.

Key words: Amyloid fibrillation, Protein denaturation, Kinetics, Nickel ion, Lysozyme

I. INTRODUCTION

Amyloid fibrillation is the misfolding process of proteins to form fibrillar aggregates with organized β-sheet-rich structures. Amyloid fibrils are regarded to be a hallmark of more than 30 major neurogenic diseases such as Alzheimer's disease (AD) and Parkinson's disease (PD) [1–4]. Hen egg white lysozyme (HEWL), containing 30% α-helix and 6% β-sheets, has 40% homology of its peptide chain amino acid sequence with human lysozyme. Due to the similar protein structure, HEWL is widely used as a prototype to study the protein denaturation [5, 6].

Increasing evidence shows that the amyloid fibrillation kinetics and the structures of the formed fibrils are closely related to environmental parameters, *e.g.*, pH [7], temperature [8], acids [9], metal ions [10, 11], and nanoparticles [12]. Specifically, relatively high concentrations of transition metal ions, such as Fe(III), Cu(II) and Zn(II), were found in amyloid plaques in the brains of AD patients, and hence a hypothesis was proposed that these metal ions can bind specifically to peptides and become factors (or cofactors) in the etiology of degenerative neurological diseases [13–15]. Therefore, the

* Authors to whom correspondence should be addressed. E-mail: xzhou@ustc.edu.cn, slliu@ustc.edu.cn

influence of metal ions on amyloid fibrils formation has attracted extensive attentions, especially to concentration effects. For instance, an inhibition effect of zinc ions in a concentration-dependent manner was reported on amyloid fibrillation of HEWL in thermal (60 °C) and acidic (pH=2.0) conditions, while morphologies of the produced amyloid fibrils were insignificantly changed [16]. The similar inhibitor role was found for copper salts in the formation of HEWL fibrils in the conditions of pH 11.8 and 37 °C [17]. Moreover, a decrease in 8-anilinonaphthalene-1-sulfonic acid (ANS) fluorescence intensity was observed with the increase of Cu(II) concentration, which was attributed to strong interactions between the ions and hydrophobic moieties of the protein [17]. By varying the NaCl and HEWL monomer concentration, the kinetic phase diagrams of the protein amyloid aggregations in pH=2 and 52 °C conditions were achieved by Muschol group [18, 19]. Three denaturation pathways were proposed by them to form fibrils, oligomers, and amorphous aggregates, depending on ionic strength. Wawer *et al.* performed a HEWL denaturation study of concentration-dependent Mg(II) and Al(III) ions in pH=2.0 and 60 °C conditions [20]. For these two metal ions, finer fibers were found to dominate at low concentrations, while proteins preferred to form amorphous aggregates at high concentrations.

Similar to Zn, Cu, and Mg elements, nickel is also an essential trace element for human body, since some physiological processes of life are closely associated with Ni(II) ions at a moderate level. It is reported that a significant excess of nickel can cause allergies, skin damage, respiratory cancers, and other problems [21–23]. Therefore, the concentration-dependent influence of Ni(II) ions is probably an important factor for understanding the related diseases. Recently, Li *et al.* claimed no observable changes in the circular dichroism (CD) spectra of HEWL and $NiCl_2$ with different concentrations in pH=4.6 aqueous solutions, indicating the insignificant transformations of protein secondary structures [24]. By detecting fluorescence intensity, Benoit *et al.* found that the addition of Zn(II) and Ni(II) ions enhanced the aggregation of Aβ40 peptide *in vitro* [25]. Jin *et al.* observed the enhanced formation of nanoscale oligomers and cytotoxicity of Aβ42 by Ni(II) ions using transmission electron microscope (TEM) approach [26]. On the contrary, some experiments showed the opposite conclusions of the Ni(II) role in protein amyloid fibrillation process. When amyloid fibrils were prepared in the presence of Ni(II) and Cu(II) ions, Fan *et al.* proposed that the metal ions could occupy functional sites of protein, leading to the production of short fibers, and as a result, an inhibitor role was suggested for the metal ions in the protein aggregation [27]. Notably, in these previous studies, scientists have paid more attentions to morphology and secondary structures of the end-formed aggregates, and the Ni(II) concentration effect in the HEWL denaturation process has never been studied. This gives us a motivation to clarify the action mechanism of Ni(II) ions on the formation kinetics of amyloid fibrils at the molecular level.

To facilitate experimental measurements, we used a relatively stressful condition of thermal (65 °C) and acidic (pH 2.0) treatment to study the HEWL amyloid fibrillation in the absence or presence of Ni(II) ions, since the overall denaturation kinetics with the thermal and acid treatment has been well-studied previously [12, 28, 29]. In this work, the secondary and tertiary structure changes of HEWL were monitors with Raman spectroscopy combined with thioflavin-T (ThT) fluorescence spectroscopy. Moreover, two representative concentrations of Ni(II) ions were utilized as 1.36 and 27.2 mmol/L (molar ratios of Ni(II) to HEWL were 1:1 and 20:1), to show the concentration dependence of HEWL amyloid fibrillation. Based on our results, the specific action of Ni(II) ions on each kinetic stages of amyloid fibril formation is illuminated.

II. MATERIALS AND METHODS

A. Preparation of HEWL solutions

HEWL in its natural state (activity ≥20,000 U/mg) was purchased from Sangon Biotech and used without further purification. The concentration of HEWL in aqueous solution was set as 20 mg/mL, and the pH value was adjusted to 2.0 using hydrochloric acid. Two Ni(II) ion concentrations, 1.36 and 27.2 mmol/L, were achieved by adding $NiCl_2{\cdot}6H_2O$ into the solutions with the molar ratio of 1:1 and 20:1 of nickel ions to HEWL, respectively. 5 mL of the solutions were packed into sealed glass vials and incubated at 65 °C in a thermostat without stirring. At specific incubation times, the protein solutions were taken out from the vials and centrifuged at 12000 g for 20 min to separate out gelatinous phase. The supernatant was used for the following spontaneous Raman spectroscopy and ThT fluores-

DOI: 10.1063/1674-0068/cjcp2303023

cence spectroscopy experiments.

B. Spontaneous Raman spectroscopy

The experimental setup of spontaneous Raman spectroscopy was described elsewhere [28, 29]. In brief, a continuous laser (Verdi V5, coherent, 532 nm, 4 W) was focused onto the solution in a 10 mm×10 mm quartz cuvette at the set temperature. Raman scattering was dispersed by a Triple monochromator (Triple-Pro, Acton Research) and detected with a liquid-nitrogen-cooled CCD detector (Spec-10:100B, Princeton Instrument). The Raman shift was carefully calibrated according to the standard spectral lines of mercury lamps and the resolution was about 1 cm^{-1}. The acquisition time of recording each spectrum was about 1 min. Under the identical conditions, Raman spectrum of each supernatant was accumulated and averaged through 10 times of collection. Finally, the reported Raman spectrum was further corrected by subtracting the spectrum of water.

C. ThT fluorescence assays

ThT dye was purchased from Sigma-Aldrich. 0.5 mL of supernatant was taken at different incubation time and added to 4.5 mL of ThT aqueous solution (concentration of 12 mg/L). With photoexcition at 409 nm, fluorescence emission spectra of the mixed solutions were recorded by a multi-purpose fiber optic spectrometer (AvaSpec-ULS2048, Avantes) in the wavelength range of 400–800 nm. The emission intensity at 477 nm was used as an indicator of ThT fluorescence intensity.

III. RESULTS AND DISCUSSION

A. Raman indicators for the secondary and tertiary structures of HEWL

Raman spectroscopy is widely applied in the protein amyloid fibrillation process, because peak position, intensity, and full width at half maximum (FWHM) of Raman vibrational bands are very sensitive to the secondary and tertiary structure transformations of proteins [30, 31]. Hereby, we record spontaneous Raman spectra of HEWL aqueous solutions at various incubation time with thermal and acidic trearment, in the range of 600–1800 cm^{-1}. According to the formation of insoluable aggregates, the protein concentration in the supernatant continues to decrease with incubation time, resulting in the reducing intensities of all Raman bands. Similar to previous experimental studies [28, 29, 32], the Raman spectra can be normalized with the peak intensity of the Phe band at 1003 cm^{-1} to eliminate the effect of protein concentration, since the Phe intensity is proportional to the protein concentration and insensitive to the microscopic environments of protein [33].

We know, tryptophan (Trp) has the most massive side chain among all amino acid residues of HEWL [34]. Thus, intense Trp bands are easily observed in its Raman spectra. Among these bands, the sharp peak at 759 cm^{-1} and the doulet one around 1340–1360 cm^{-1} are often used as the indicators of the protein tertiary structure transformations [31]. Notably, the peak at 759 cm^{-1} is attributed to in-phase symmetric breathing vibration of the benzene and pyrrole ring of the indole group, so-called the W18 mode, thus, its band width is sensitive to the conformational distributions of Trp residues on side chain [33, 35]. Moreover, the doublet at 1340 cm^{-1} and 1360 cm^{-1} is assigned to the W7 mode of protein as the Fermi resonance between in-plane N1=C8 vibrational fundamental band and one or more combined bands of out-of-plane vibrations [36]. The ratio of this doublet intensity (I_{1340}/I_{1360}) is a sensitive probe for the hydrophobic/hydrophilic environment around Trp residues. When the I_{1340}/I_{1360} value is less than 1, the Trp residues are in hydrophobic surrounding or in contact with aliphatic side chains. On the contrary, they are located in hydrophilic environment or exposed to aqueous media [31].

For protein secondary structures, the N–C_α–C peak at 933 cm^{-1} and the amide I band in the range of 1640–1680 cm^{-1} are two commonly used indicators. Because the peak at 933 cm^{-1} is exclusively contributed by the N–C_α–C stretching vibration of α-helices [37], its band intensity is a sensitive marker to the content of α-helices. In comparison, the amide I band includes rich information of protein strucutres, as different secondary structures have slightly different peak positions in this wavenumber range, *e.g.*, α-helix is usually located at 1650–1660 cm^{-1} [38], β-sheets are at 1671–1673 cm^{-1} [28, 33, 39], β-turns and random structures are in 1670–1680 cm^{-1} [40], extended PP II in protofiber is at 1667 cm^{-1} [41], β-intermolecular and intramolecular structures are located at 1669 and 1682 cm^{-1}, respectively [42].

FIG. 1 shows the recorded Raman spectra of HEWL in the native state (in black) and the end-formed products (after incubation for 196 h) in the presence of Ni(II) ions at two concentrations of 1.36 mmol/L (in

DOI: 10.1063/1674-0068/cjcp2303023

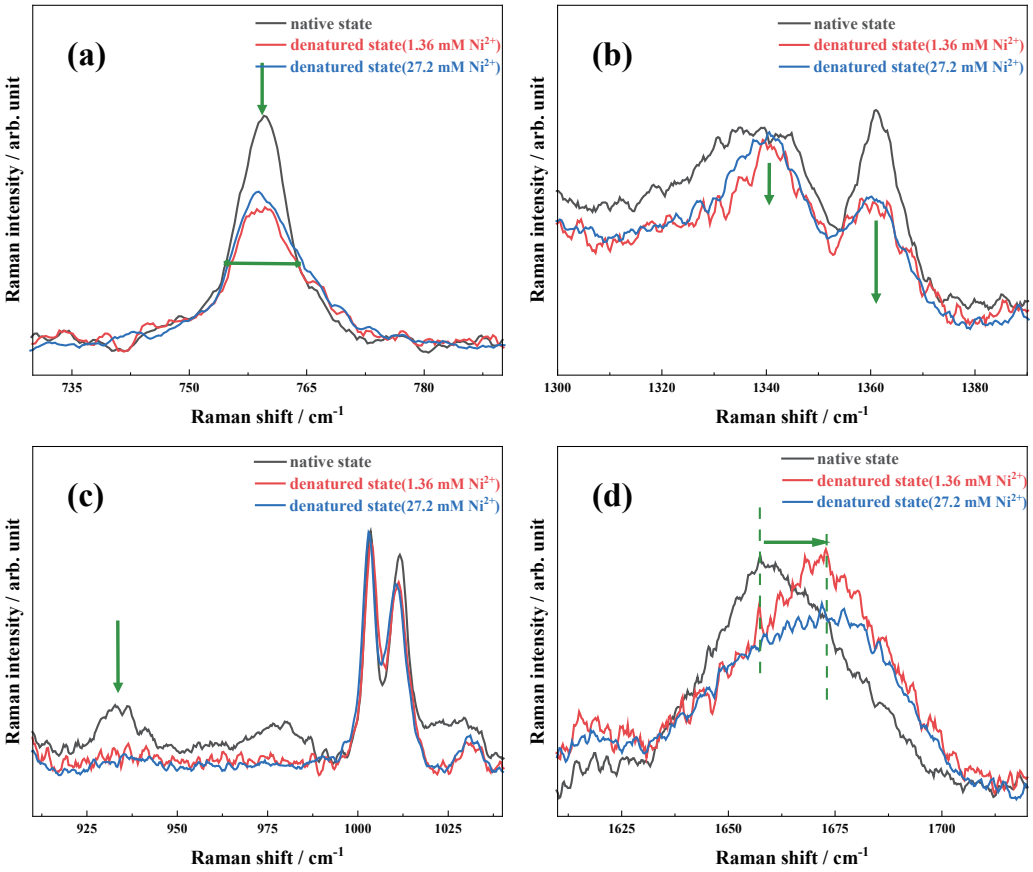

FIG. 1 Raman spectra of the native HEWL (in black) and the end-formed products in the presence of Ni(II) ions at the concentration of 1.36 mmol/L (in red) and 27.2 mmol/L (in blue) in the range of 730–790 cm^{-1} (a), 1300–1390 cm^{-1} (b), 910–1040 cm^{-1} (c), and 1610–1720 cm^{-1} (d), with thermal and acidic treatment.

red) and 27.2 mmol/L (in blue) in thermal and acid conditions, respectively. We must emphasize that the incubation time of 196 h is sufficient to complete the amyloid fibrillation process in current experimental conditions [28, 29, 32]. As indicated previously [28, 29], the predominant denatured products are mature fibers with cross β-sheet-rich structures in thermal and acidic conditions. Notably, there is no obvious change for the native HEWL in the presence and absence of Ni(II) ions (not shown in FIG. 1), indicating insignificant influence of Ni(II) ions on the initial molecular structures of lysozyme. In contrast, the four Raman bands exhibit distinct changes after long-time incubation with the action of Ni(II) ions as shown in FIG. 1, implying the occurance of secondary and tertiary structure transformations in protein amyloid fibrillation. In addition, the changes for these four indicators show a positive correlation with the Ni(II) concentration, that is, the more significant variation is observed in Raman spectra with the increase of Ni(II) concentration.

For simplicity, only results at high concentration of 27.2 mmol/L Ni(II) are described here as a representative. The FWHM of the Trp band at 759 cm^{-1} is broadened from 7.4 cm^{-1} in the native state to 11 cm^{-1} in the final state for HEWL, as shown in FIG. 1(a). Thus, the more conformations of Trp residues exist in the HEWL denatured products induced by the Ni(II) ions. Similarly, the I_{1340}/I_{1360} ratio is increased to larger than 1 after long-time incubation (FIG. 1(b)), indicating a change of hydrophobic-to-hydrophilic microenvironment around the Trp side chains. For the secondary structures, the band intensity at 933 cm^{-1} decreases significantly and almost completely disappears (FIG. 1(c)), providing solid evidence for destruction of the α-helix structures of HEWL in the denatured state. Moreover, the peak position of amide I band is visibly blue-shifted by 16 cm^{-1}, as exhibited in FIG. 1(d). According to the spectral assignments mentioned above, β-sheets are definitely formed.

B. Unfolding kinetics of the HEWL tertiary structures

The amyloid fibrillation of HEWL is well-known as a

DOI: 10.1063/1674-0068/cjcp2303023

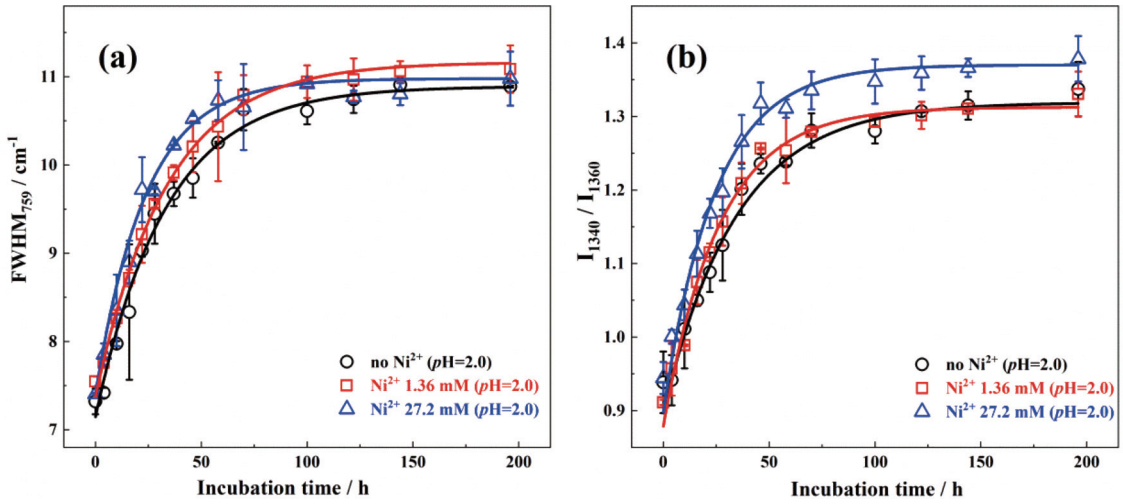

FIG. 2 The incubation time-dependence curves of the FWHM at 759 cm^{-1} (a) and the I_{1340}/I_{1360} ratio (b) in the absence (in black) and presence of Ni(II) ions at the concentration of 1.36 mmol/L (in red) and 27.2 mmol/L (in blue) with thermal and acidic treatment.

multi-stage process along with an outside-in mechanism in thermal and acidic conditions [17, 28]. In other words, the unfolding of protein tertiary structures prefers to occurring prior to the changes of secondary structures due to interactions between inducers and active groups on protein surface [17, 28]. Along this mechanism, we paid attention to the specific influence of Ni(II) ions in each stage, such as the unfolding kinetics of tertiary strucutres and the transformation of secondary structures.

FIG. 2(a) shows the incubation time-dependence curves of the FWHM at 759 cm^{-1} in the three experimental conditions. Apparently, three curves all exhibit single exponential growth, indicating that the unfolding of tertiary structures immediately occurs. In other words, these incubation conditions are very efficient for initiating protein denaturation. Moreover, according to that the rate of rise in the presence of Ni(II) ions at low concentration is close to that without the metal ions, the determinant factor in this process mainly originates from acid. However, the grown process is slightly accelerated with the action of Ni(II) ions at the high concentration, affirming the promotor role of the metal ions on the unfolding kinetics of tertiary strucutres on protein surface. As shown in FIG. 2(b), the I_{1340}/I_{1360} indicator exhibits the similar kinetic behavior, which increases progressively with incubation time regardless of the presence of nickel ions. This kinetics clearly manifests the exposure of Trp residues on side chains to hydrophilic environment. In addition, the growth rate of the I_{1340}/I_{1360} ratio is obviously accelerated with the increasing Ni(II) concentration (FIG. 2(b)). Based on the kinetics of the two indicators, Ni(II) ions show a concentration-dependent promotor role in the unfolding kinetics of HEWL tertiary strucutres.

C. Transformation kinetics of the HEWL secondary structures

Since mature fibers are of organized β-sheet-rich structures, the secondary structures of HEWL must transform from the initially dominant α-helix to organized β-sheets during amyloid fibrillation process. Thus, the incubation time-dependence curves of two Raman indicators, the N–C_α–C band intensity at 933 cm^{-1} and the peak position of amide I band, are presented in FIG. 3.

To uncover the Ni(II) influence on the kinetics of protein secondary structure transformation, three experimental results with thermal/acid, thermal/acid/low concentration Ni(II), and thermal/acid/high concentration Ni(II) are directly compared in FIG. 3. Overall, the kinetic behaviors of the two Raman indicators show the similar incubation time-dependence. The N–C_α–C peak intensity decreases monotonically and almost disappears within ~60 h, regardless of the presence and concentration of Ni(II) ions. Moreover, the degradation rate of the α-helices with the three treatments are approximately equal, implying that Ni(II) ions have minor influence on the α-helix depletion of HEWL or much less than the effect of acid.

In general, most protein amyloid fibrillation occurs through a nucleation dependent mechanism, such as

DOI: 10.1063/1674-0068/cjcp2303023

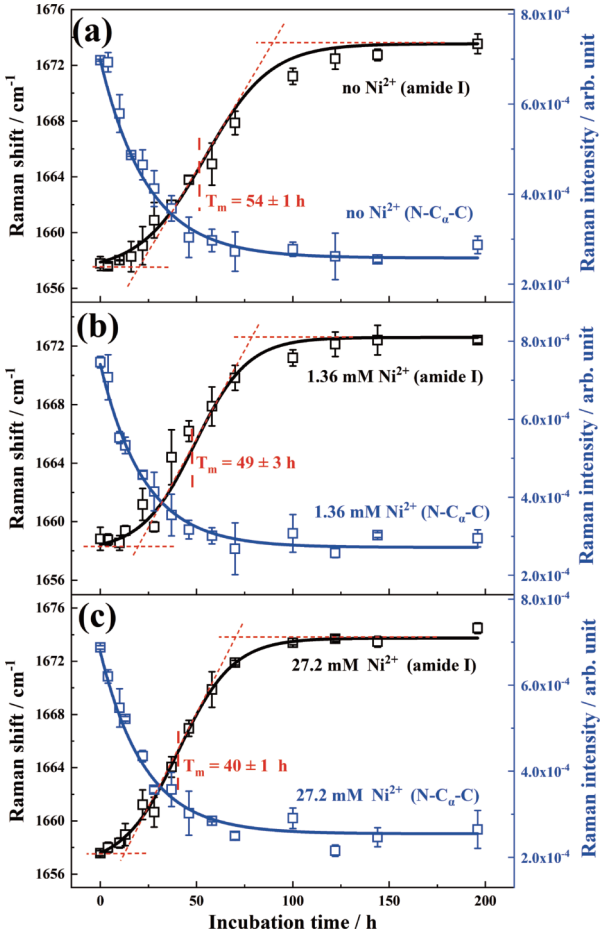

FIG. 3 Incubation time-dependent curves of the N–C_α–C stretching band intensity at 933 cm^{-1} and the peak position of amide I band, in the absence (a) and in the presence of Ni(II) ions at the concentration of 1.36 mmol/L (b) and 27.2 mmol/L (c) with thermal and acidic treatment.

HEWL, whose kinetic process generally follows a sigmoidal function that goes through three successive stages: a lag phase, a growth phase and an equilibrium phase [43, 44]. Obviously, a typical sigmoidal dependence is also achieved for the peak position of the amide I band in the three conditions, as shown with black curves in FIG. 3. In order to obtain detailed kinetic parameters for comparison, we fitted these kinetic curves with the following Eq.(1), which is usually to describe changes in amyloid fibrillation over time, such as the fluorescence intensity [45–49],

$$F = F_{\mathrm{D}} + \frac{F_{\mathrm{N}} - F_{\mathrm{D}}}{1 + \exp\left(\dfrac{T - T_{\mathrm{m}}}{\Delta T}\right)} \tag{1}$$

where F_{N} and F_{D} are the peak positions of the initial and final states, respectively, T is the incubation time, T_{m} is the transition midpoint of the sigmoid curve, and

TABLE I The lag duration (T_0), transition midpoint time (T_{m}), equilibrium duration (T_{e}), and a half interval (ΔT) of the peak position of the amide I indicator in the HEWL amyloid fibrillation process with thermal and acidic treatment.

[Ni(II)]/(mmol/L)	T_0/h	T_{m}/h	T_{e}/h	ΔT/h
0	21	54±1	89	16
1.36	19	49±3	79	14
27.2	13	40±1	71	14

$2\Delta T$ represents the transition time interval. In addition, two parameters. T_0 and T_{e} are defined to quantitative represent of the lag duration and the time to reach equilibium state, respectively; as shown in FIG. 3, they can be approximatively determined as the cross points between the fitted lines of the lag and the growth phase, and the growth and the equilibrium phases, respectively. Table I summarizes the derived T_{m}, T_0 and T_{e} values of this Raman indicator in the three conditions.

According to the known amyloid fibrillation mechanism in thermal and acidic condition [28], soluble oligomers are preferentially produced with unfolding of protein tertiary structures, then they aggregate to form a nucleus during the lag phase, followed by assembly of the nuclear template protein to fibrils. Therefore, a two-step mechanism of protein secondary structure transformations is generally accepted that α-helix prefers to transform into statistical coils, then these random coils gradually assemble to organized β-sheets [28]. As shown in FIG. 3 and Table I, the lag duration is significantly shortened with the addition of Ni(II) ions, and moreover, the degree of shortening becomes more pronounced with increasing concentration. In addition, it is worthy noting that the most α-helices are destroyed within ~60 h (FIG. 3), and the amide I peak position is approximately blue-shifted to its maximum in this time due to the action of Ni(II) ions at high concentration (FIG. 3(c)). These results strongly imply that the Ni(II) ions have an efficiently accelerating effect on the HEWL secondary structure transformation. More specifically, the direct transformation from α-helix to β-sheets by skipping the formation of intermediate statistical coils can occur due to the action of metal ions.

Additionally, the metal ion influence shows a positive concentration-dependent characterestics. In other words, the promotion action of Ni(II) ions is enhanced with its concentration. To futher study this specific influence, the amide I band profiles of the denatured state in the three conditions are directly compared in FIG. 4.

DOI: 10.1063/1674-0068/cjcp2303023

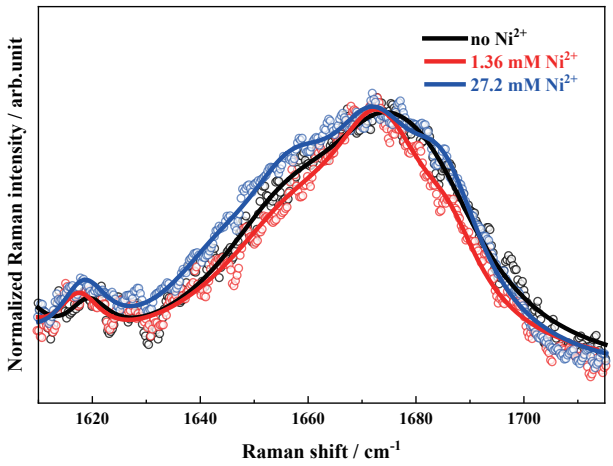

FIG. 4 Normalized amide I band profiles of HEWL in the denatured states in the absence (in black) and in the presence of Ni(II) ions at the concentrations of 1.36 mmol/L (in red) and 27.2 mmol/L (in blue) in thermal and acidic conditions.

Apparently, the band profiles are visibly changed with the addition of Ni(II) ions. A narrower band width is observed in comparison with that without the metal ions in the case of the low concentration of Ni(II) ions. The components with the Raman shift at lower than 1600 cm^{-1} and higher than 1680 cm^{-1} are reduced as shown in the red trace of FIG. 4. According to the aforementioned assignments of different secondary structures, less β-intramolecular structures (with the Raman shift at >1680 cm^{-1}) are formed and the organized β-sheets are more predominant. This indicates that Ni(II) ions play an efficient role in the HEWL amyloid fibril formation. However, the influence becomes more complicated when the Ni(II) concentration is increased to a higher level (such as 27.2 mmol/L). The spectral profile is significantly broadened as shown in the blue curve of FIG. 4, even wider than that in the absence of metal ions. As we know, only the contributions of α-helix, extended PP II in protofiber and β-intermolecular structures are located at lower than 1670 cm^{-1}. Almost α-helical structures are destroyed in protein denaturation process as indicated by the N–C_α–C marker at 933 cm^{-1}. Thus, the observed broadened peak profile strongly implies that more extended PP II and β-intermolecular structures exist in the end-formed state with the action of Ni(II) ions at high concentration. That is, the Ni(II) ions at high concentration accelerate the transformation of HEWL secondary structures, but more disordered structures are formed in assembly of soluble oligomers and nuclear template protein with too fast aggregating rate.

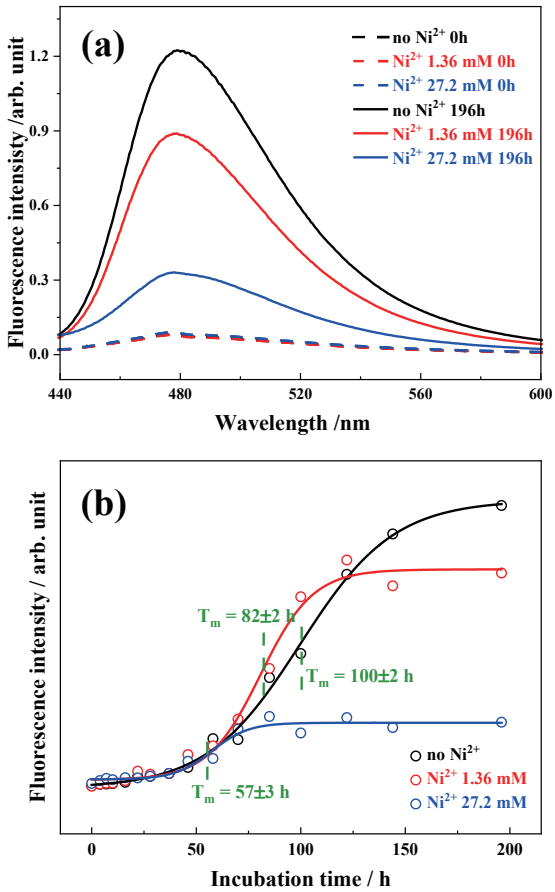

FIG. 5 (a) Fluorescence spectra of HEWL and ThT mixed solution in the native state and denaturation state after incubation for 196 h with thermal/acid (in black), thermal/acid/Ni(II) treatments ($[Ni^{2+}]$ of 1.36 mmol/L in red, 27.2 mmol/L in blue); (b) incubation time-dependence of the ThT fluorescence intensity at 477 nm.

D. ThT fluorescence assays

Due to the spectral overlap of various secondary structures in the amide I band, it is difficult to accurately quantify the amount of β-sheet using Raman spectroscopy. Notably, it is well known that ThT fluorescence intensity can be significantly enhanced by binding to organized β-sheets, so that ThT fluorescence assay is widely used to quantify organized β-sheet structure as a gold standard [50, 51].

FIG. 5(a) shows the ThT fluorescence spectra of the HEWL solutions in the native and final states, in the absence and presence of Ni(II) ions. Obviously, the fluorescence intensity is enhanced after protein denaturation. However, to our surprise, the Ni(II) concentration exhibits a negative correlation with the enhancement effect, *i.e.* the increase factor of ThT fluorescence intensity is remarkably reduced with increasing Ni(II) concentration. This trend looks opposite to the accelerator

DOI: 10.1063/1674-0068/cjcp2303023

role of the metal ions indicated by Raman spectroscopy.

To further uncover its influence, the incubation time-dependence of the ThT fluorescence intensity at 477 nm is plotted in FIG. 5(b). All kinetic curves are typical sigmoidal-function relationship. Thus, we fitted these variations with the Eq.(1) [48, 49] and the fitting curves are also shown in FIG. 5(b). The transition midpoint T_m is determined to be 100±2 h in the absence of metal ions, 82±2 h with the addition of Ni(II) ions at 1.36 mmol/L, and 57±3 h in the presence of Ni(II) ions at high concentration of 27.2 mmol/L. The decrease of the T_m value with increasing concentration of the metal ion affirms the promotion influence of Ni(II) ions on the HEWL amyloid fibrillation, which greatly agrees with the above conclusion of Raman spectroscopy.

Besides, since the ThT fluorescence intensity is sensitive to the content of organized β-sheet structures in the denaturaed protein, its reducing intensity at equilibrium state in comparison with that without metal ions indicates that the assembly of soluble oligomers and nuclear template protein into other aggregates with disordered structures is significantly promoted by Ni(II) ions.

IV. CONCLUSION

In this study, Raman spectroscopy was used to study the concentration effect of Ni(II) ions on kinetics of the HEWL amyloid fibrillation in thermal and acidic conditions at the molecular level. The unfolding kinetics of protein tertiary structures were monitored by two Raman indicators, the Trp band intensity at 759 cm^{-1} and the Fermi doublet of Trp residues at 1340 and 1360 cm^{-1}. The accelerated viaration rate in the presence of Ni(II) ions indicates the accelerator effect of Ni(II) ions. Similarly, we performed an investigation on the secondary structure transformation of HEWL in the addition of Ni(II) ions. Using the N–C_α–C band intensity at 933 cm^{-1} and the peak position of amide I band (1640–1680 cm^{-1}) as the Raman indicators, we recorded the corresponding evolution kinetics. All experimental evidence indicates that Ni(II) ions can promote the direct transformation of α-helices to others, even skipping the formation of intermediate statistical coils. Moreover, the accelerating effect of Ni(II) ions is found to be concentration-dependent.

Using the ThT fluorescence assays, the content of β-sheets in the HEWL amyloid fibrillation with thermal/acid and thermal/acid/Ni(II) treatments was quantified. Interestingly, a negative effect on the formation of fibrils with organized β-sheets was found for Ni(II) ions as an inhibitor, because the more significantly promotion influence is validated on the assembly into other aggregates with disordered structures. These results provide rich information about the specific metal-mediated protein fibrillation.

V. ACKNOWLEDGEMENTS

This work was financially supported by the National Natural Science Foundation of China (No.22073088, No.22027801 and No. 21873089).

[1] F. Chiti and C. M. Dobson, Annu. Rev. Biochem. **86**, 27 (2017).
[2] R. N. Rambaran and L. C. Serpell, Prion **2**, 112 (2008).
[3] K. A. Conway, J. D. Harper, and P. T. Lansbury, Biochemistry **39**, 2552 (2000).
[4] C. M. Dobson, Nature **426**, 884 (2003).
[5] C. Redfield and C. M. Dobson, Biochemistry **29**, 7201 (1990).
[6] R. Swaminathan, V. K. Ravi, S. Kumar, M. V. S. Kumar, and N. Chandra, Adv. Protein Chem. Struct. Biol. **84**, 63 (2011).
[7] H. Wang, J. Wu, R. Sternke-Hoffmann, W. Zheng, C. Morman, and J. Luo, Commun. Chem. **5**, 171 (2022).
[8] S. Y. Ow and D. E. Dunstan, Soft Matter **9**, 9692 (2013).
[9] N. A. Jamuna, A. Kamalakshan, B. R. Dandekar, A. M. Chittilappilly Devassy, J. Mondal, and S. Mandal, J. Phys. Chem. B **127**, 2198 (2023).
[10] P. Faller, C. Hureau, and O. Berthoumieu, Inorg. Chem. **52**, 12193 (2013).
[11] J. Sheng, N. K. Olrichs, W. J. Geerts, D. V. Kaloyanova, and J. B. Helms, Sci. Rep. **9**, 1 (2019).
[12] M. Konar, A. Mathew, and S. Dasgupta, ACS Omega **4**, 1015 (2019).
[13] J. A. Duce and A. I. Bush, Prog. Neurobiol. **92**, 1 (2010).
[14] L. M. Miller, Q. Wang, T. P. Telivala, R. J. Smith, A. Lanzirotti, and J. Miklossy, J. Struct. Biol. **155**, 30 (2006).
[15] M. A. Lovell, J. D. Robertson, W. J. Teesdale, J. L. Campbell, and W. R. Markesbery, J. Neurol. Sci. **158**, 47 (1998).
[16] B. Ma, F. Zhang, X. Wang, and X. Zhu, Int. J. Biol. Macromol. **98**, 717 (2017).
[17] R. Ceron, M. Peimbert, A. Rojo-Dominguez, and H.

Najera, J. Biomol. Struct. Dyn. **41**, 423 (2023).
[18] S. E. Hill, T. Miti, T. Richmond, and M. Muschol, PLoS One **6**, e18171 (2011).
[19] T. Miti, M. Mulaj, J. D. Schmit, and M. Muschol, Biomacromolecules **16**, 326 (2015).
[20] J. Wawer, M. Szocinski, M. Olszewski, R. Piatek, M. Naczk, and J. Krakowiak, Int. J. Biol. Macromol. **121**, 63 (2019).
[21] B. Zambelli, V. N. Uversky, and S. Ciurli, Biochim. Biophys. Acta **1864**, 1714 (2016).
[22] J. Zhao, X. Shi, V. Castranova, and M. Ding, J. Environ. Pathol. Toxicol. Oncol. **28**, 177 (2009).
[23] G. Drochioiu, M. Manea, M. Dragusanu, M. Murariu, E. S. Dragan, B. A. Petre, G. Mezo, and M. Przybylski, Biophys. Chem **144**, 9 (2009).
[24] S. J. Li, A. Nakagawa, and T. Tsukihara, Biochem. Biophys. Res. Commun. **324**, 529 (2004).
[25] S. L. Benoit and R. J. Maier, Sci. Rep. **11**, 1 (2021).
[26] L. Jin, W. H. Wu, Q. Y. Li, Y. F. Zhao, and Y. M. Li, Nanoscale **3**, 4746 (2011).
[27] Y. Fan, H. Lan, Z. Qi, R. Liu, and C. Hu, Chemosphere **297**, 134241 (2022).
[28] L. Xing, W. Fan, N. Chen, M. Li, X. Zhou, and S. Liu, J. Raman Spectrosc. **50**, 629 (2019).
[29] L. Xing, N. Chen, W. Fan, M. Li, X. Zhou, and S. Liu, Int. J. Biol. Macromol. **132**, 929 (2019).
[30] A. Rygula, K. Majzner, K. M. Marzec, A. Kaczor, M. Pilarczyk, and M. Baranska, J. Raman Spectrosc. **44**, 1061 (2013).
[31] N. Kuhar, S. Sil, and S. Umapathy, Spectrochim. Acta Part A **258**, 119712 (2021).
[32] W. Fan, L. Xing, N. Chen, X. Zhou, Y. Yu, and S. Liu, J. Phys. Chem. B **123**, 8057 (2019).
[33] S. Dolui, A. Mondal, A. Roy, U. Pal, S. Das, A. Saha, and N. C. Maiti, J. Phys. Chem. B **124**, 50 (2020).
[34] M. R. R. de Planque, B. B. Bonev, J. A. A. Demmers, D. V. Greathouse, R. E. Koeppe, F. Separovic, A. Watts, and J. A. Killian, Biochemistry **42**, 5341 (2003).
[35] J. A. Sweeney and S. A. Asher, J. Phys. Chem. **94**, 4784 (1990).
[36] I. Harada, T. Miura, and H. Takeuchi, Spectrochim. Acta Part A **42**, 307 (1986).
[37] V. Kocherbitov, J. Latynis, A. Misiunas, J. Barauskas, and G. Niaura, J. Phys. Chem. B **117**, 4981 (2013).
[38] A. Barth, Biochim. Biophys. Acta **1767**, 1073 (2007).
[39] S. Dolui, A. Roy, U. Pal, A. Saha, and N. C. Maiti, ACS Omega **3**, 2452 (2018).
[40] A. Barth and C. Zscherp, Q. Rev. Biophys. **35**, 369 (2002).
[41] K. Huang, N. C. Maiti, N. B. Phillips, P. R. Carey, and M. A. Weiss, Biochemistry **45**, 10278 (2006).
[42] S. Mangialardo, F. Piccirilli, A. Perucchi, P. Dore, and P. Postorino, J. Raman Spectros. **43**, 692 (2012).
[43] P. Ghosh and P. De, ACS Appl. Bio. Mater. **3**, 9598 (2020).
[44] C. C. Lee, A. Nayak, A. Sethuraman, G. Belfort, and G. J. McRae, Biophys. J. **92**, 3448 (2007).
[45] L. Nielsen, R. Khurana, A. Coats, S. Frokjaer, J. Brange, S. Vyas, V. N. Uversky, and A. L. Fink, Biochemistry **40**, 6036 (2001).
[46] A. Chaari, C. Fahy, A. Chevillot-Biraud, and M. Rholam, PLoS One **10**, e0142095 (2015).
[47] X. Chen, X. Deng, X. Han, Y. Liang, Z. Meng, R. Liu, W. Su, H. Zhu, and T. Fu, ACS Omega **6**, 3307 (2021).
[48] B. S. Moorthy, H. T. Ghomi, M. A. Lill, and E. M. Topp, Biophys. J. **108**, 937 (2015).
[49] S. Karmakar, N. Sarkar, and L. M. Pandey, Colloids Surf. B **174**, 401 (2019).
[50] H. Levine, Protein Sci. **2**, 404 (1993).
[51] M. Biancalana and S. Koide, Biochim. Biophys. Acta **1804**, 1405 (2010).

DOI: 10.1063/1674-0068/cjcp2303023